Article

Not peer-reviewed version

Scratch Resistance of a Plasma-Assisted Duplex Treated 17–4 Ph Stainless Steel Additively Manufactured by Laser Powder Bed Fusion

Arturo Gómez-Ortega , Julián Andrés Pinilla-Bedoya , Carolina Ortega-Portilla , Christian Félix-Martínez ,
Guillermo César Mondragón-Rodríguez , Diego Germán Espinosa Arbeláez , James Pérez-Barrera ,
Juan Manuel González-Carmona * , Edgar Adrián Franco Urquiza

Posted Date: 26 March 2024

doi: 10.20944/preprints202403.1517.v1

Keywords: 17-4 PH stainless steel; additive manufacturing; DUPLEX treatment; hardness; scratch resistance

Preprints.org is a free multidiscipline platform providing preprint service that is dedicated to making early versions of research outputs permanently available and citable. Preprints posted at Preprints.org appear in Web of Science, Crossref, Google Scholar, Scilit, Europe PMC.

Copyright: This is an open access article distributed under the Creative Commons Attribution License which permits unrestricted use, distribution, and reproduction in any medium, provided the original work is properly cited.

Preprints.org (www.preprints.org) | NOT PEER-REVIEWED | Posted: 26 March 2024

doi:10.20944/preprints202403.1517.v1

Disclaimer/Publisher's Note: The statements, opinions, and data contained in all publications are solely those of the individual author(s) and contributor(s) and not of MDPI and/or the editor(s). MDPI and/or the editor(s) disclaim responsibility for any injury to people or property resulting from any ideas, methods, instructions, or products referred to in the content.

Article

Scratch Resistance of a Plasma-Assisted DUPLEX Treated 17-4 PH Stainless Steel Additively Manufactured by Laser Powder Bed Fusion

Arturo Gómez-Ortega [1], Julián Andrés Pinilla-Bedoya [2], Carolina Ortega-Portilla [1], Christian Félix-Martínez [1], Guillermo César Mondragón-Rodríguez [1], Diego Germán Espinosa Arbeláez [1], James Pérez-Barrera [1,3], Juan Manuel González-Carmona [1,*] and Edgar Adrián Franco Urquiza [1]

[1] CONAHCYT-Centro de Ingeniería y Desarrollo Industrial, CIDESI, Querétaro, Av. Pie de la Cuesta 702, Querétaro 76125, México.
[2] CONAHCYT-Cinvestav, Libramiento Norponiente 2000, Fraccionamiento Real de Juriquilla, Querétaro 76230, México.
[3] Current address: Departamento de Termofluidos, Facultad de ingeniería, Universidad Nacional Autónoma de México (UNAM), CDMX 04510, México.
* Correspondence: juan.gonzalez@cidesi.edu.mx; Tel.: +52 442 748 0070

Abstract: Additive manufacturing (AM) or 3D printing of metals is gaining popularity due to its flexibility in fabricating parts with highly complex designs, as well as simplifying manufacturing steps and optimizing process times. In this investigation, 17-4 PH stainless steel was additively manufactured using Laser-Powder Bed Fusion (L-PBF), followed by functionalization through a DUPLEX treatment. This treatment involved a plasma-assisted nitriding process, followed by deposition of an arc-PVD c-$Al_{0.7}Cr_{0.3}N$ hard coating. The microstructural modifications resulting from plasma nitriding (such as the formation of $Fe_{2,3}N$ and Fe_4N, and the α_N or expanded martensite phases), and the surface improvements with the c-$Al_{0.7}Cr_{0.3}N$ coating on the 3D-printed 17-4 PH steel, are evaluated in comparison to conventionally manufactured 17-4 PH steel. These microstructural characteristics are correlated with the mechanical response of the treated surfaces. As a result of the plasma nitriding process, the hardness of the 3D-printed 17-4 PH SS increased by approximately 260%. The wear, measured through dynamic and static scratch-testing, was reduced by approximately 31%. This improvement was attributed to the modification of adhesive failure mechanisms, leading to a reduction in wear volume, improved coating adhesion, and enhanced scratch resistance.

Keywords: 17-4 PH stainless steel; additive manufacturing; DUPLEX treatment; hardness; scratch resistance

1. Introduction

Additive manufacturing (AM), or 3D printing of metallic parts, has grown in popularity due to its ability to fabricate parts with highly complex designs. Additionally, AM simplifies the manufacturing steps in the production cycle and optimizes processing times [1]. Industries such as aerospace, biomedical, automotive, tooling, among others, are exploring AM as a production process to develop optimal components in form and functionality. The most popular AM process for metals is Laser-Powder Bed Fusion (L-PBF), in which 3D parts are built by the superposition of micro-layers of powder melted selectively. L-PBF is a mature technology with an increasing variety of metallic powder alloys ready to use [2]. However, parts produced by L-PBF may have bulk and surface defects inherent to the printing process, necessitating different post-processing steps (e.g., nitriding, carburizing, thermal aging, and coating deposition, among others) to achieve the desired characteristic properties and functionalities before their industrial implementation [3]. In any case, any post-processing or surface functionalization needs to be evaluated to assess its pertinence and practical perspectives.

© 2024 by the author(s). Distributed under a Creative Commons CC BY license.

Preprints.org (www.preprints.org) | NOT PEER-REVIEWED | Posted: 26 March 2024 doi:10.20944/preprints202403.1517.v1

Among the most commonly used and essential alloys for mankind, Stainless Steels (SS) have been widely employed in several applications and sectors: manufacturing tools, biomedical instruments and prostheses, chemistry, food processing, brewing, heat exchange, engine parts, valves, etc. Nowadays, methods for producing and processing conventional SS parts may include various hot and cold forming steps. However, in order to reduce the number of processing steps or to manufacture SS parts and prototypes with highly complex geometries, AM technologies have become the solution of choice [4]. Using optimal processing conditions, AM might produce materials with better properties, such as the 17-4 PH SS, where printed specimens have displayed better wear resistance under dry conditions compared to forged 17-4 PH SS samples [5]. The goal is to develop AM parts with the same properties or even better than conventional manufacturing methods [6]. Precipitation-Hardened (PH) SS is applied as structural materials where corrosion resistance is needed, such as in salt-rich environments, oil and gas, power plants, and chemical industries. This is due to their excellent balance between mechanical properties and corrosion resistance, stemming from their high copper and chromium content. They are commonly used in various applications at working temperatures below 300°C. The microstructure of 17-4 PH SS is characterized by the precipitation of copper-rich phases in a martensitic matrix [7]. Concerning AM 17-4 PH SS parts, they have shown good mechanical and corrosion properties in their as-built conditions [8, 9], fabricated by Selective Laser Melting (SLM) [10, 11], laser deposition, and supersonic laser deposition [12].

One method to improve the properties of metallic surfaces is by locally hardening them through plasma nitriding, which can be further enhanced with the deposition of a hard coating produced by physical vapor deposition (PVD) techniques. The combination of both processes is called the DUPLEX treatment. The main advantage of the plasma nitriding process is the low treatment temperatures (< 450 °C), which prevent substrate microstructural degradation and allow for an increase in surface hardness due to nitrogen diffusion in the alloy, leading to the formation of expanded crystalline phases and stable iron nitrides. Additionally, the geometric, dimensional, and surface finish effects on the substrate are negligible [13, 14].

Moreover, PVD hard coatings allow for substantial improvements in surface properties, such as hardness and wear resistance. Furthermore, the dimensional modifications of the coated part(s) fall within the range of thicknesses (< 5 μm) of the protective layers. Therefore, applying a DUPLEX treatment results in a hardness gradient that increases the mechanical properties, wear resistance, and lifetime of the part during service. [15, 16]. Literature reports indicate that wrought 17-4 PH SS has been successfully nitrided from relatively thin depths (2.4 to 23.4 μm) [17] to depths above 100 μm in gas activated and plasma-assisted processes (DC and pulsed) with temperatures ranging from 350 to 500 °C [18-22]. However, when the nitriding treatment takes place at temperatures higher than 400°C for extended periods (more than 4 hours), overaging may occur, resulting in detrimental outcomes. For instance, this may involve the formation of an external white layer (consisting of a mixture of $Fe_{2,3}N$ and Fe_4N nitrides) and the outward diffusion of chromium to form a brittle CrN layer with low adhesion. Such effects can be detrimental to the mechanical properties of the coating-steel surface system [22].

Based on this, the thermal treatment history (e.g., aged, solution treated) of the SS will have a critical effect on the characteristics of the nitrided layer and the bulk properties [23]. Additionally, the nitriding conditions will affect the adhesion and performance of any coating deposited on it [24]. To date, the effects of surface treatments, such as the plasma-assisted nitriding process applied to 3D printed 17-4 PH SS, have not been reported. Information on the effects of plasma nitriding on additively manufactured 17-4 PH SS is essential for material selection and application design.

L-PBF AM is likely to produce refined grains and introduce local defects such as porosities or lack-of-fusion, resulting in a rough surface finish that affects the mechanical and wear properties of the 3D-printed structure [25]. Hence, the surface finishing and hardening with the DUPLEX treatment presented and discussed in this research can contribute to a large number of applications and parts manufactured by AM for various industrial purposes.

In this work, a DUPLEX treatment consisting of plasma nitriding followed by $Al_{0.7}Cr_{0.3}N$ arc-PVD coating was applied to 3D-printed 17-4 PH SS coupons fabricated using the L-PBF method. The first part of this document discusses the effects of the surface treatments on the evolution of crystalline phases and the microstructure of the steel surface. In the second part, these analyses are correlated with the surface hardness and scratch resistance of the 3D-printed 17-4 PH SS and the nitrided + coated system.

2. Materials and Methods

2.1. Additive Manufacturing of 17-4 PH SS

Morphology and chemical composition of the 17-4 PH SS powders (Concept Laser, GE Additive) were obtained using field-emission scanning electron microscopy coupled with an energy dispersive spectroscopy probe (FE-SEM/EDS) in a Jeol JSM-7200F equipped with an Ultim max 100 EDS probe from oxford instruments. The particle size distribution was obtained in a Sympatec Helos LD system, equipped with a Rodos R2 dry module using a 0.2 bar of pressure. Figure 1a shows the FE-SEM image of the 17-4 PH SS powder particles with roughly spherical morphology, peanut-like agglomerated grains, and the sporadic appearance of pores. Particle size and cumulative distribution in figure 1b, showed that the distribution proved to be monomodal with a D_{10} = 17.63 μm, D_{50} = 26.34 μm, and D_{90} = 34.76 μm.

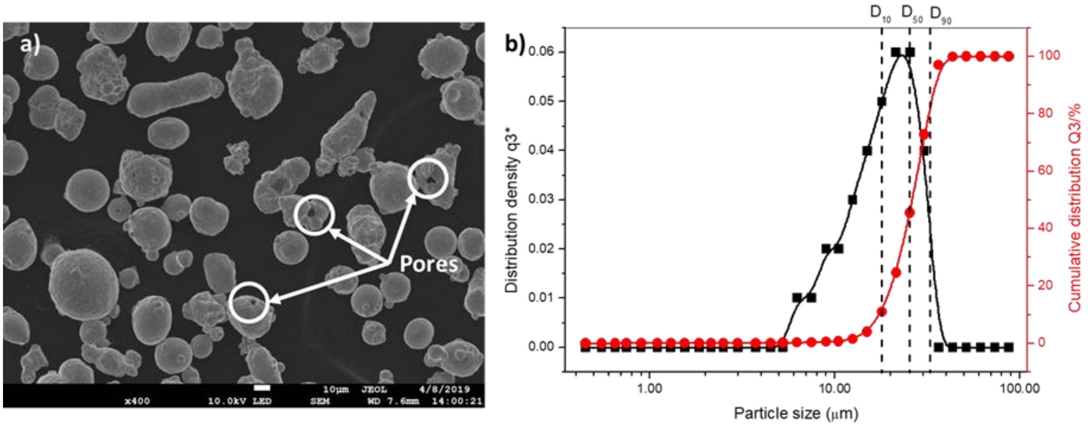

Figure 1. (a) 17-4 PH steel powder morphology and (b) Particle size and cumulative distribution obtained by laser diffraction.

AM 17-4 PH SS was manufactured under a nitrogen environment in a Laser-Powder Bed Fusion system (L-PBF) M2 Cusing Multilaser from Concept Laser. The laser power was 370 W, a scanning speed of 800 mm/s with a scan pattern of random 5 × 5 mm square islands, a laser spot size of 135 μm, and a hatch distance (trace spacing) of 0.12 mm, for a layer thickness of 25 μm. Rectangular rods of 10 × 10 × 50 mm were printed. As-built samples were cut along the XY-plane (perpendicular to the printing direction) using a diamond disc to obtain 5 mm thick samples. Likewise, a 2.54 cm diameter commercially forged bar of 17-4 PH steel was obtained, then cut into 5 mm height sections. Both materials (L-PBF and forged) were heat treated using the H900 procedure to increase resistance and obtain an equivalent microstructure [26]. Before the DUPLEX treatment, the L-PBF and forged samples were polished down to mirror finish using 3 μm Al_2O_3 suspension by standard metallography procedures. To evaluate the microstructure, samples were chemical-etched using Fry's etchant (5g $CuCl_2$ + 40ml HCl + 25ml ethanol + 30ml distilled H_2O) and then characterized by FE-SEM.

2.2. The DUPLEX Treatment

DUPLEX treatment was performed in a Domino Mini PVD coater from Oerlikon, which consists of a plasma nitriding step followed by the deposition of an arc-PVD $Al_{0.7}Cr_{0.3}N$ (hereafter called AlCrN). The plasma nitriding was conducted using an Arc Enhanced Glow Discharge (AEGD)

Preprints.org (www.preprints.org) | NOT PEER-REVIEWED | Posted: 26 March 2024 doi:10.20944/preprints202403.1517.v1

process [27]. Initially, samples were ultrasonically cleaned, mounted in the two-fold rotation holder and placed into the reactor chamber. Rotation speed was kept to 2 Hz for the complete DUPLEX process. Subsequently, a 10^{-3} Pa vacuum was obtained, followed by a 2 h heating stage at ~ 350 °C. Plasma cleaning in Ar atmosphere (1 Pa) at 250 V RF bias, 20 kHz, and 80 % active time was applied for 25 min to activate the forged and L-PBF surfaces. The plasma nitriding was achieved using an 80 % active RF shielded cathodic arc (AEGD) with 80 A, 20 kHz, 1 Pa, and a mixture of 278 sccm Ar + 50 sccm N_2 + 25 sccm H_2 high purity gasses, the process was applied for 90 min. AlCrN films were deposited by plasma-assisted cathodic arc using Al/Cr alloy targets (70/30 at.%) from PLANSEE, with 150 A, working pressure of 0.4 Pa, 500 sccm N_2 flow, and a substrate temperature of ~ 430 °C kept constant throughout the deposition process. A -80 V Bias voltage and a total of 45 min were used to obtain a final coating thickness of ~ 1.3 μm.

2.3. Material Characterization

In order to study the crystalline structure and phase evolution through the different processing steps, i.e., heat treated, and plasma nitrided, and DUPLEX coated, the Grazing Incidence X-ray diffraction (GI-XRD) technique was used. As a reference, XRD patterns from the steel powder were also obtained. GI-XRD was performed using a Rigaku Smartlab diffractometer with a CuKα source (λ = 1.5406 Å), an incidence angle of 2°, 0.04° step and a period of 10 sec/step were used.

Thicknesses and microstructures of the nitrided layers and coatings were estimated from the cross-sections by FE-SEM, tracking the nitrogen signal using an EDS line strategy (100 single spectra in a 37 μm length line beginning from the surface). The nitrided layer was correlated with the determination of the Vickers micro-hardness using a 3 N load and 10 s dwell time obtained with a Revetest RST3 Indenter from Anton Paar. The mechanical properties of the coating were obtained by nanoindentation, using a Fischer HM200 equipment with 300 mN load.

2.4. Scratch Resistance

In order to study the adhesion and scratch resistance of the AlCrN coating in the DUPLEX treatment, dynamic and static scratch tests were performed using a diamond Rockwell C indenter (Φ = 200 μm). Dynamic tests were performed using a load gradient from 0 to 35 N at a 3.5 mm distance. Critical loads and scratch tracks were evaluated using FE-SEM and compared to the ASTM C 1624-05 standard. Static tests were performed using constant loads of 15 and 23 N in a 3.5 mm distance. In order to estimate the loss volume, 3D profiles were generated in an olympus DSX 5000 confocal microscopy using a 50X lens. Subsequently, the wear coefficient was obtained using the Archard model [28]. Finally, to evaluate the scratch resistance, the static tests were carried out on the AM and forged steel before and after the DUPLEX treatment.

3. Results and Discussion

3.1. Chemical and Microstructural Analysis

Table 1 shows the chemical composition obtained by EDS from the steel powder, the top surface of forged and AM 17-4 PH SS samples after heat treatment, and the nominal composition provided by Concept Laser. The elemental composition after printing is in good agreement with its feedstock powder, except for the silicon composition, which shows a higher percentage for the forged sample and a lower percentage for the steel obtained by AM. The percentage of niobium, phosphorous and sulfur are also higher in the forged sample compared to the powder and 3D printed material. Powder composition control is essential for the final properties of the printed parts, and its variation during fabrication will affect the final microstructure and therefore their mechanical properties [29].

Table 1. Chemical composition of the 17-4 PH stainless steel powder, forged, L-PBF and the nominal composition provided by Concept Laser.

Element	Initial Powder (wt. %)	Forged (wt. %)	L -PBF (wt. %)	Nominal Composition from Concept laser (wt. %)
Si	0.45	0.88	0.28	1
P	0.04	0.24	<0.01	0.04
S	0.02	0.36	<0.01	0-0.03
Cr	16.16	15.72	16.5	15-17.5
Mn	0.8	1.34	0.98	1
Ni	3.80	4.39	3.71	3-5
Cu	3.75	3.10	3.45	3-5
Nb	0.25	1.07	0.3	0.15-0.45
Fe	69.3	72.90	69.62	Balance

A representative microstructure of the forged and additively manufactured samples after H900 heat treatment and etching with Fry's reagent are shown in figure 2. Fine martensite grains and austenitic structures located at the grain boundaries are observed. These observations are consistent with other bibliographic reports, where it has been shown that due to the rapid cooling of the L-PBF process, it is possible to obtain retained austenite at the grain boundaries [30-32]. However, the refinement of martensite grains due to heat treatment was more homogeneous in the material obtained by AM than in the forged material. This is evident as the austenite grains observed in Figure 2a are larger, irregular, and more abundant compared to those observed in Figure 2b. This effect is caused because the additive manufacturing process melts material selectively, with high cooling rates, which can cause the distribution of alloys to not be distributed homogeneously in the material [29-33]. However, it is observed that the microstructures obtained are equivalent.

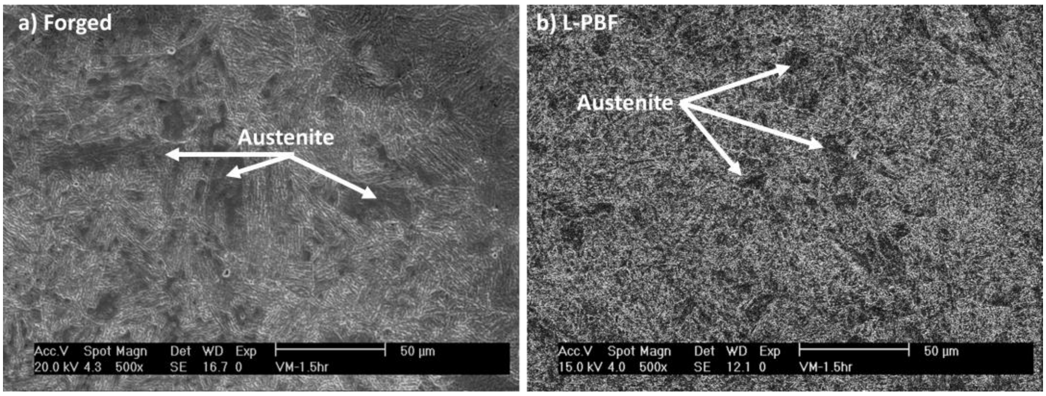

Figure 2. Microstructure of the 17-4 PH SS alloy after heat treatment a) forged and b) printed by L-PBF.

3.2. Crystalline Phase Identification

Figure 3a compares the GI-XRD patterns of the 17-4 PH feedstock powder, AM samples, forged, both after heat treatment and plasma nitrided samples. Results showed that both the α-Fe phase (bcc-martensite) and some traces of the γ-Fe phase (fcc-austenite) are present in the feedstock powder, in the L-PBf and the forged material. As shown in Figure 2, γ phase is visible as micrometer-sized clusters, mainly at the martensitic grains boundaries and was observed to be more abundant in the forged material. After the plasma-assisted nitriding process, $Fe_{2,3}N$ and Fe_4N phases were formed due to the chemical reactions taking place between the N-ions and the steel. Additionally, an increase in the FWHM and a shift to lower 2θ angles of the initial α peaks are observed, see Figure 3b. This behavior has been observed by different researchers and corresponds to the N-ions diffusion into the bcc structure, forming an expanded martensite phase (EM) or αN [17, 19, 20]. Furthermore, the diffraction peak intensity at $2\theta = 43.6°$ increases due to the formation of the Fe_4N phase. Formation of the γ phase due to the nitriding process (350 °C, 2-h) can be ruled out because no diffraction peaks were identified for this phase. Since aging temperatures for the 17-4 PH SS are relatively low, with short exposure times (e.g., 482 °C for 1-h), some researchers have investigated the pertinence of performing thermal treatments together with the plasma nitriding, finding that it is possible to obtain uniform microstructures extending the nitriding time. However, it was reported that under certain conditions, an external chromium nitride (CrN) layer is formed, which is fragile and tends to spall off, being a detrimental side effect of the dual-purpose treatment [17]; although, other treatment conditions exhibited benefits to fatigue life under high-stress conditions [21]. On the other hand, Sun and Bell [34] reported the precipitation of CrN after plasma nitriding at 430 °C; however, the features in their GI-XRD patterns indicate that the CrN formation might start at 425 °C or slightly lower temperatures.

In our case, the presence of the CrN phase was not detected by GI-XRD. This indicates that the nitriding process did not achieve critical N-concentrations to stabilize internal nitride precipitates or an external nitride layer.

Figure 3c shows the GI-XRD pattern for the AlCrN coating obtained after cathodic arc evaporation, which is consistent with an fcc structure with an Fm3m space group, showing the diffraction peaks (111), (200), (220), and (311). The material corresponds to a solid solution between elements Al and Cr in a B1-NaCl configuration, no peaks from the binary nitrides (e.g., AlN-wurtzite and Cr_2N-Hexagonal) were found. The diffraction pattern shows preferential orientation in the (111) plane, which belongs to the densest plane of the fcc structure; however, high-intensity peaks were also observed in the (200) and (220) orientations. This is a consequence of the high energy involved in the cathodic arc deposition process, where atoms tend to be located such that the free energy of the system is minimized, and high energy species tend to be arranged in planes with less density (or less residual stress). The dependence of the crystalline orientation in PVD-coatings has been extensively studied for different deposition methods, having ion density, bias voltage, and pressure as main parameters [35, 36].

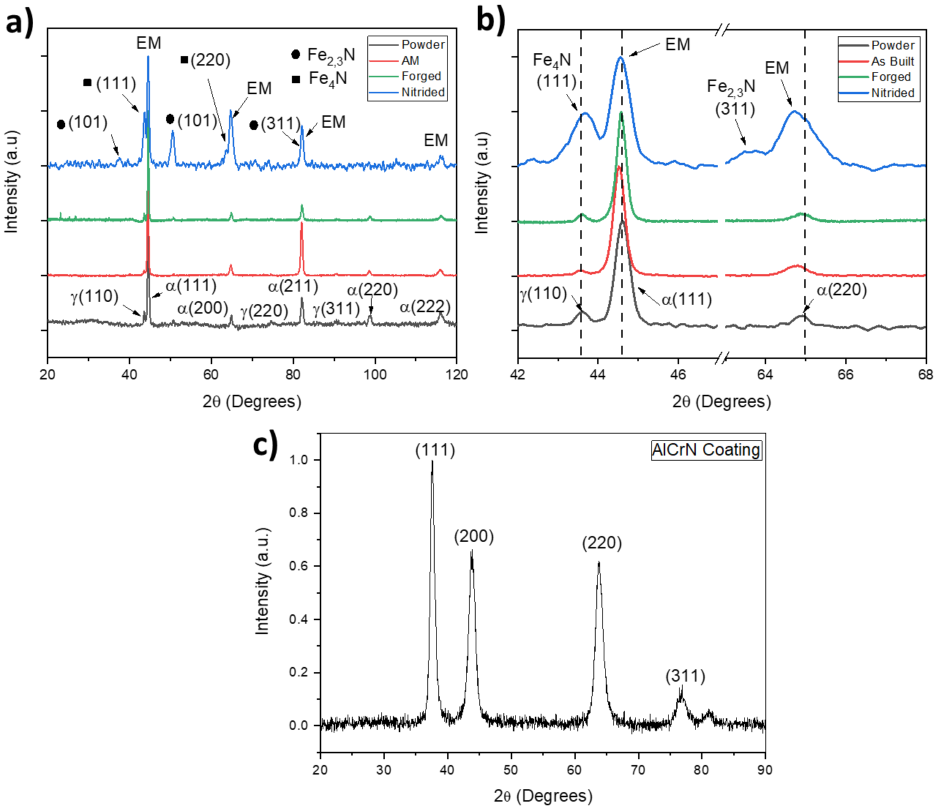

Figure 3. Grazing incidence X-ray diffraction patterns for a) 17-4 PH SS powder, 3D-printed sample, forged sample, and plasma nitrided, b) a zoom-in view for peaks between 42 and 68°, and c) AlCrN coating deposited by cathodic arc.

3.3. Cross-Sectional Characterization after the DUPLEX Treatment

Figures 4a and 4b show the cross-section of the steel manufactured by L-PBF and forged after the DUPLEX treatment respectively. The formation of a homogeneous diffusion layer of around 26.5 µm for the AM material and 21.38 µm for forged material was observed. No nitride segregation was visible after Fry's reagent etching at steel grain boundaries, showing a homogenous nitrogen diffusion. Figure 4c shows the AlCrN coating, with a typical morphology of zone II in the Thornton diagram, composed of columnar grain growth and well-defined grain boundaries with no visible porosity. However, the formation of microdroplets of the molten material from the target is observed on the coating surface, which is characteristic of the cathodic arc deposition process [37, 38]. The variation in nitrogen content along the cross-section (Figure 4d) (i.e., dotted line of Figure 4a and b), shows a zone rich in nitrogen for both materials, corresponding to the diffusion layer, which shows variations between 6.9 and 5.4 wt%, followed by a rapid reduction of the element until reaching zero nitrogen content. This reduction is more abrupt for the forged material, which is due to a smaller interface between the steel core and the nitrided layer.

Other authors have reported nitrided layers for 17-4 PH SS of 5 and 23 µm thickness for plasma-assisted nitriding processes at temperatures of 400°C for 20 h and 500°C for 5 h, respectively [17, 18]. On the contrary, the high density of ions generated by the arc Enhanced Glow Discharge (AEGD) process results in greater efficiency compared to conventional plasma-assisted nitriding, allowing for layer thicknesses higher than 20 µm to be obtained at temperatures below the annealing temperature of the steel (~350°C). Additionally, short nitriding times (1.5 h) prevent the formation of Cr-depleted zones and the formation of CrN precipitates, which have been reported to increase surface fragility and reduce fatigue resistance [18].

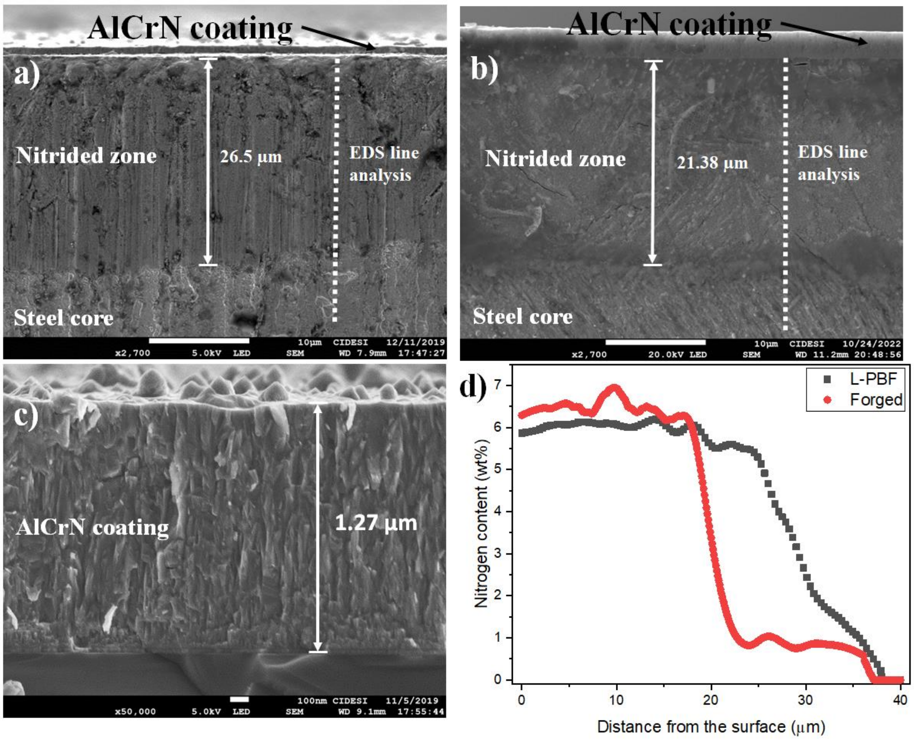

Figure 4. a) FE-SEM cross-section image of the DUPLEX treated AM steel, b) FE-SEM cross-section image of the DUPLEX treated forged steel, c) cross-section of the DUPLEX treatment and d) nitrogen content as a function of the distance from the surface obtained by EDS from the nitrided zone.

Preprints.org (www.preprints.org) | NOT PEER-REVIEWED | Posted: 26 March 2024 doi:10.20944/preprints202403.1517.v1

3.4. Hardness Analysis after the DUPLEX Treatment

Figure 5 shows the hardness profile obtained from the nitrided 3D-printed 17-4 PH steel and the forged steel cross-section. An increase of ~ 2.5 times in hardness was achieved in the outer zone (~ 26.5 μm), with a maximum value for the L-PBF of 857 ± 20 and 752 ± 18 $HV_{0.01}$ for the forged steel, which agrees with the nitrided region (figure 4a and b). Subsequently, a sudden decrease in hardness is observed until the average value of the 3D printed 17-4 PH steel (328 ± 8 HV) and the forged steel core (348 ± 12 HV) are reached. The higher bulk hardness of the steel obtained by forging in comparison with the steel obtained by additive manufacturing is due to the differences in microstructure observed in figure 2. Furthermore, the hardness of the c-AlCrN coating obtained by nanoindentation was 15.63 GPa (~ 2897 HV), and the elastic modulus of 415.58 GPa. These results showed that with the DUPLEX treatment, the surface hardness increases more than 2 times with respect to the nitriding case and ~9 times concerning the steel substrate, which agrees with the literature reports for similar treatments [39-41]. The microstructure and hardness measurements allow us to state that through the DUPLEX treatment, a gradient of mechanical properties has been generated, which will act as a load-bearing buffer during the life-service of the material.

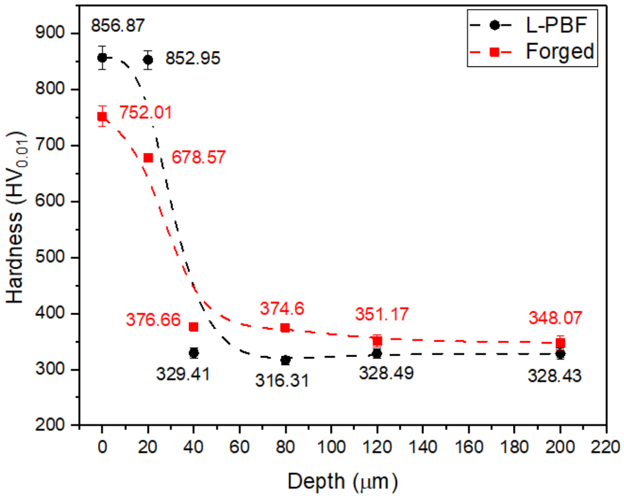

Figure 5. Vickers Hardness from the cross-section of the 3D-printed and forged 17-4 PH steel after plasma nitriding.

The abrupt drop in hardness implies a diffuse nitrogen concentration gradient with a rapid reduction of the element, consistent with what was observed in the composition profile performed by EDS in Figure 4d. Additionally, it is possible to relate it to the asymmetry (increase in the FWHM and a shift to lower 2θ angles) observed in the peaks of expanded martensite in the diffraction patterns (Figures 3a and b). The broadening and asymmetric shift of the EM peaks indicate the inclusion of nitrogen at the surface of the material and diffusion towards the α-Fe matrix, resulting in a nitrogen concentration gradient from the unaffected steel substrate towards the surface.

3.5. Scratch Resistance of the DUPLEX - 3D Printed 17-4 HP SS

Dynamic scratch testing

The adhesion of a coating is widely recognized as the most critical characteristic, as its relevance in any application is diminished if the material fails to adhere to the substrate. To delve into this essential property, we employed the dynamic scratching technique. This method enabled us to explore two pivotal aspects: the cohesive and adhesive loads at critical points (Lc1 & Lc2) and the overall separation of the coating, which correlates with the ultimate critical load (Lc3). Figure 6 shows the representative curves of the drag coefficient, including the load and acoustic signal versus the scratch distance for the forged/duplex (figure 6a) and the L-PBF/duplex (figure 6b).

The first observable peaks associated with cohesive failures (Lc1) appear at ~7 ± 2 N for forge/DUPLEX and ~12 ±3 N for L-PBF/DUPLEX (these values are averaged from 3 separated measurements). Which corresponds to the formation of the first cracks on the surface. Subsequently, peaks with high relative acoustic emission intensity associated with the critical adhesive load (Lc2) are observed for both systems at Lc2 ~ 15 ± 3 N for the forged (figure 6a) and Lc2 ~ 21 ± 2 N for the LPBF DUPLEX (figure 6b). Changes in acoustic emission are also reflected in changes in the drag coefficient, however these changes can be subtle and difficult to interpret. For this reason, it is essential to analyze the scratch tracks, through the observation of the failure mechanisms and the comparison with the atlas in the ASTM C 1624-05 standard.

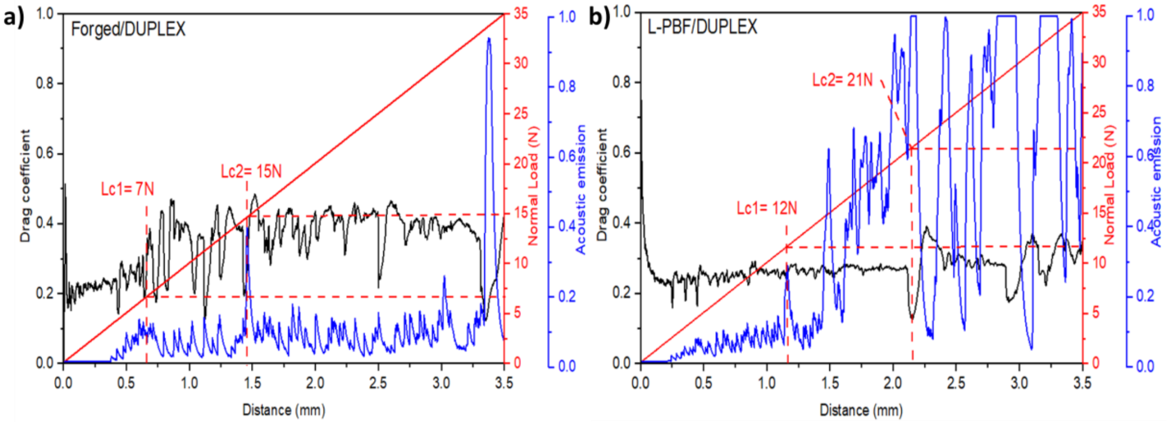

Figure 6. a. Drag coefficients (black lines), load (red lines), and acoustic emissions (blue lines) versus scratch distance for forge/duplex and b) for L-PBF/duplex.

Figure 7 shows selected areas of the scratch tracks of both substrates, at the distances where the critical loads were found. For the forged/DUPLEX (figure 7a), cohesive failure was related to forward chevron tensile cracks, which are generated on the back of the indenter due to tensile stress. For LPBF/DUPLEX (figure 7b) the cohesive failures corresponds to chevron compression cracks. This type of failures are generated in the front of the indenter due to compression stress and they reflect the plastic deformation of the substrate and the coating's attempt to accommodate this deformation. Cohesive failures are intrinsically related to the mechanical properties of the surface. Although the hardness of the coating and nitriding are similar for both systems, the forged steel showed a slightly higher hardness than the steel obtained by AM and therefore, the appearance of cracks related to brittle failures, such as cracks generated by tensile stress, will tend to appear more frequently in forged steel.

In the case of the adhesive failures (figures 7c & d), the formation of chipping spallation was observed, which is characterized by rounded-like shape areas removed from the coating in the lateral regions of the scratch track. This type of failures are related to a brittle behavior in the steel, since the coating spallation in these areas occurs by the adhesive failure of the nitrided region of the steel substrate [42, 43]. Figures 7e and 7f compare the end of the scratch-track for forged/DUPLEX and the LPBF/DUPLEX treated materials, respectively, gross spallation is observed due to high residual stresses [16, 43]. These are characterized by large sections of detached coating within and extending beyond the track and are denominated as the final critical load or Lc3, which were observed at loads of 32 ± 4 N y 30 ± 5 N for the forged/DUPLEX and the LPBF/DUPLEX respectively. In the forged/DUPLEX steel system, the appearance of buckling-type spaces is also observed, where coating buckles ahead of the indenter, producing irregularly-spaced patches missing from the coating, opening away from the direction of scratching (figure 7e)

Both coating systems showed good adhesion, with cohesive failures composed of cracks and mild adhesive failures. Serious failures, such as chevron, chipping and gross spallation, occurred after the appearance of adhesive damages, where indenter penetration increases and coating spallation is inevitable. This failure mechanism is accompanied by high-intensity peaks in the acoustic emission signal, as shown in Figure 6.

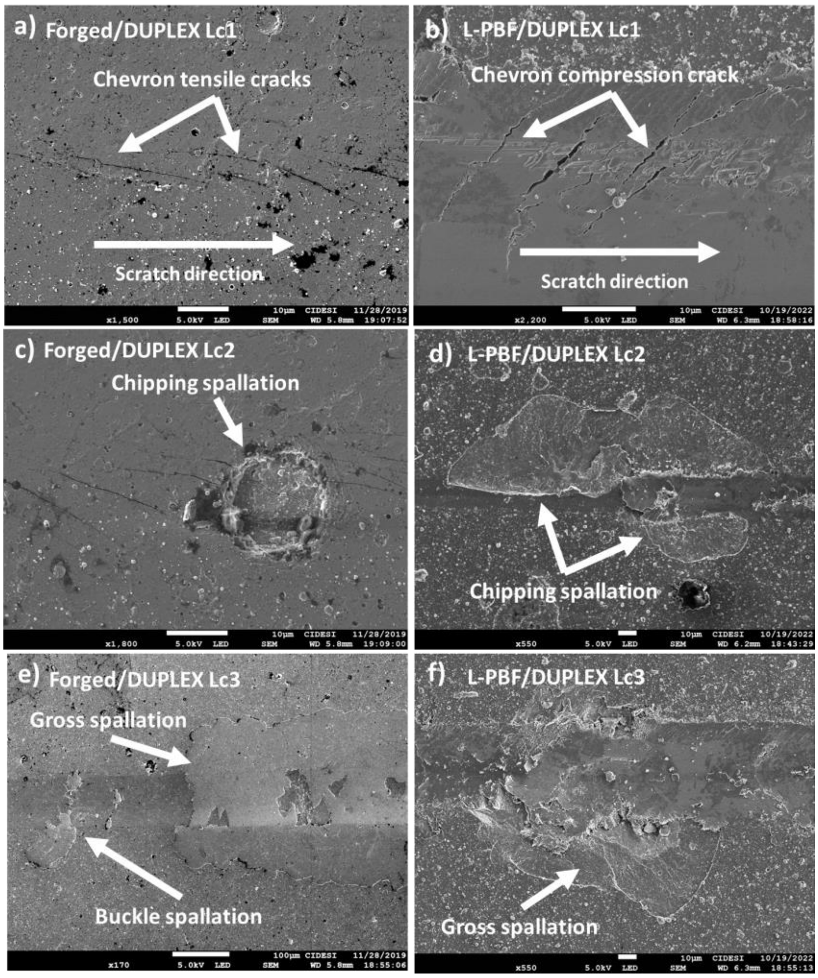

Figure 7. Selected areas of the scratch tracks at the distances where failures were obtained: a) forged/DUPLEX Lc1, b) L-PBF/DUPLEX Lc1, c) forged/DUPLEX Lc2, d) L-PBF/DUPLEX Lc2, e) forged/DUPLEX Lc3 and f) L-PBF/DUPLEX Lc3.

Static scratch resistance

In order to evaluate the scratch resistance of both the forge and LPBF, static scratch tests were performed at two normal loads, 15 N and 23 N (see Figure 8). These loads were chosen due to the behavior of the critical loads observed in Figure 6, since they are above the limit of the critical adhesion load of both systems.

Regardless of the load used, the surfaces showed a similar behavior, the 17-4 PH SS obtained by forging showed the highest and most unstable coefficient of friction (COF) of the set, with values between 0.17 and 0.25, while the 17-4 PH SS obtained by AM showed a more stable behavior, with a COF between 0.14 and 0.17. The slight increase in hardness observed for forged steel (figure 5) and the appearance of retained austenite grains after heat treatment (figure 2a) increase the friction coefficient and produce higher instabilities during scratching, while the fine microstructure observed for the steel obtained by AM (figure 2b) allowed the variation in the COF to be minor.

After the DUPLEX treatment, a reduction and increase in the stability of the COF was observed for both steels. The forged steel showed a COF with values of 0.13 and 0.16 for 15 and 23 N respectively, while the steel obtained by AM showed a COF between 0.09 and 0.11 for 15 and 23 N respectively. The increase in the mechanical properties and the ability to withstand the load of the surfaces after the DUPLEX treatment allowed a clear reduction in the COF, demonstrating the synergy presented between the plasma nitriding assisted by AEGD and the AlCrN coating.

Preprints.org (www.preprints.org) | NOT PEER-REVIEWED | Posted: 26 March 2024 doi:10.20944/preprints202403.1517.v1

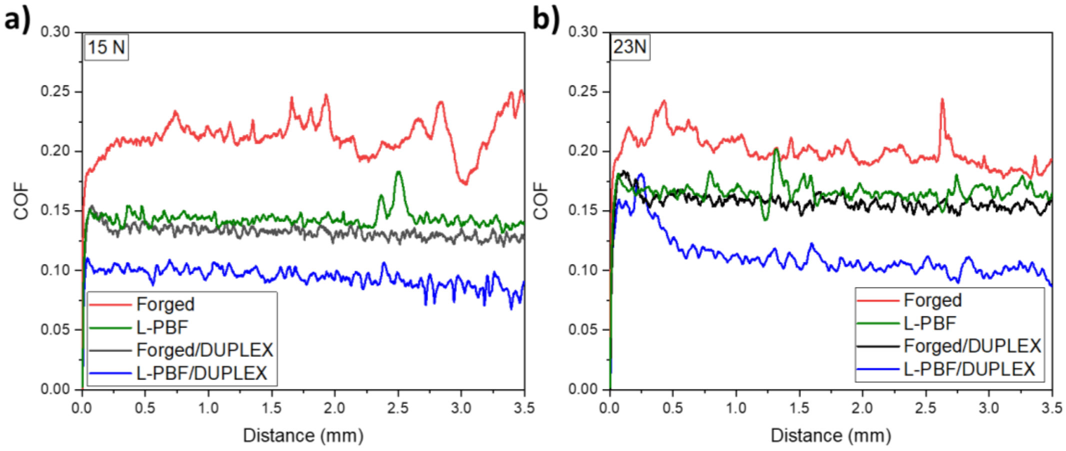

Figure 8. Static scratch test results showing friction coefficient vs distance for a) 15N constant load and b) 23N constant load.

Figure 9 shows images of the scratch tracks using confocal optical microscopy for the 23N static scratch test. Wear tracks of the L-PBF and forged steel (figures 9a & b) are wider and deeper, with a large amount of material accumulated at the edge of the track. This type of behavior is typical of materials with a relatively low plastic deformation resistance [40], which is characteristic of metals alloys. It is important to remark that the AlCrN coating deposition (figure 9c & d) increases the surface roughness of the coated system; however, thinner and shallower scratch-tracks are observed, which implies a reduction in the lost volume. Additionally, for both L-PBF and forged steel conditions, areas where the steel substrate has been plastically deformed are observed, showing a sudden increase in the width of the scratch track. For the DUPLEX treatment, zones that are practically free of discontinuities are observed in figures 9c and d. This behavior agrees with the observations made in Figure 8, where before the DUPLEX treatment, instabilities appear in the COF, characterized by sudden peaks, which are caused by plastic deformation of the substrate and the accumulation of material in the corners of the scratch track. Meanwhile, the DUPLEX treatments showed stable COF throughout the entire scratching distance.

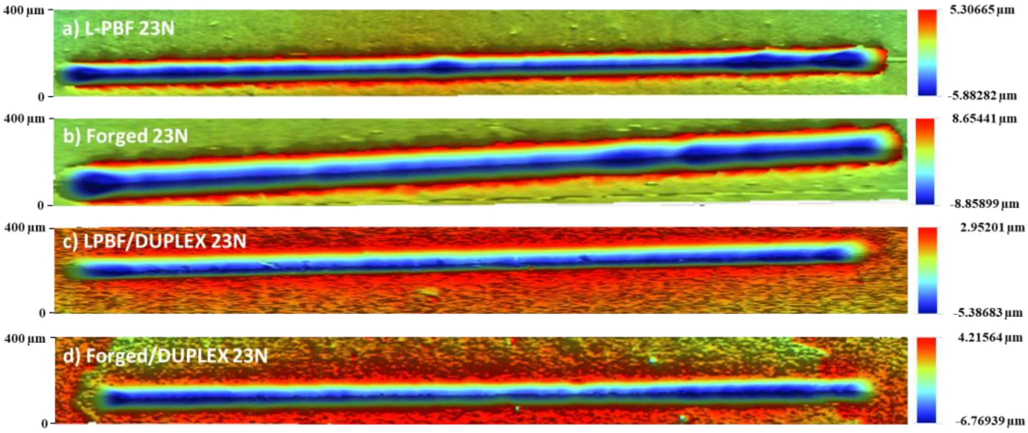

Figure 9. Confocal optical microscopy of the scratch track for: a) L-PBF 23 N, b) Forged 23 N, c) LPBF/DUPLEX 23 N and d) Forged/DUPLEX 23 N.

The wear coefficient (k) values were calculated using the worn volume (V) obtained from confocal microscopy and using the Archard model [28]:

$$k = V/Ld$$

where L is the applied load and d is the scratch distance.

Preprints.org (www.preprints.org) | NOT PEER-REVIEWED | Posted: 26 March 2024 doi:10.20944/preprints202403.1517.v1

Figure 10 shows the wear coefficients for the forged and AM 17-4 PHH SS heat treated and DUPLEX conditions. The thermally treated forged steel exhibits the highest wear coefficient, followed by the steel obtained by AM. However, upon applying the DUPLEX treatment, a decrease in the wear coefficient was observed for both materials, with reductions between 27% and 31% for forged steel and between 21% and 25% for steel produced by AM. The defects observed in the scratch tracks through confocal microscopy, which are related to the plastic deformation of the steel and lead to the appearance of instabilities in the COF, resulted in an increase in the material worn volume and, consequently, in the wear coefficient. Furthermore, the formation of a hardness gradient generated by the diffusion of nitrogen and the formation of iron nitrides in the nitriding process, which increases the intrinsic stress in both the substrate, the interface, and the deposited AlCrN layer, allows the surface to better distribute the stresses during scratching and reduce wear [44, 45].

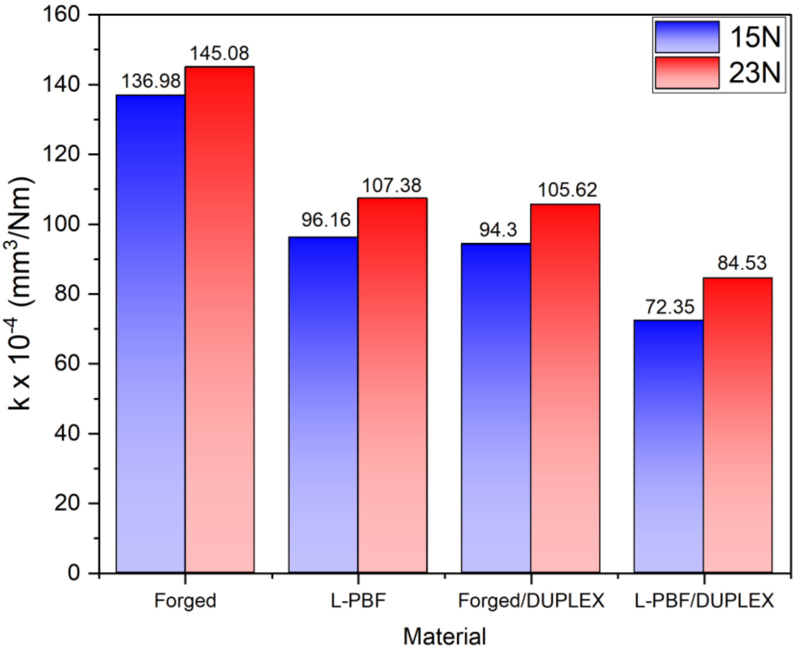

Figure 10. Wear coefficients of the forged and AM 17-4 PHH SS heat treated and DUPLEX conditions.

4. Conclusions

- The heat distribution during the printing process and the thermal history significantly influenced the microstructure of the steel after heat treatment. In the steel obtained by AM, a fine distribution of austenite grains was observed, with small sporadic zones of retained austenite, whereas the forged steel exhibited less refined austenite grains, with the presence of large grains of retained austenite. These differences directly impacted the mechanical properties of the materials, resulting in an observed increase in surface hardness for the forged material.
- After DUPLEX treatment, the formation of iron nitrides, the appearance of the expanded phase and the reduction of the gamma phase of iron were observed. For the nitriding conditions used, the appearance of segregated Cr-N phases was not observed, which can increase brittleness and reduce fatigue resistance. The thickness of the nitrided layers was between 21 and 26 um, demonstrating the high efficiency of the low-temperature AEGD-assisted nitriding process. Similarly, the growth of a homogeneous AlCrN layer of 1.27 um thickness was observed, composed of microdroplets, typical of the cathodic evaporation process by electric arc.
- The creation of a hardness gradient on the surface was observed when producing the DUPLEX treatment. The nitriding process increased the hardness of the heat-treated steel by between 210 and 260%. While the AlCrN coating increased the hardness of the substrate by 830% and 338% with respect to the nitrided surface.

- It was demonstrated that the coatings exhibited acceptable adhesion; however, differences in failure modes were observed, which were related to mechanical properties. The steel manufactured by AM presented cohesive failures related to compression mechanisms and plastic deformation. The forged steel showed failures related to brittle mechanisms induced by tension. However, the adhesive failure patterns were similar for both materials and were characterized by the appearance of chippings, indicated by rounded areas where the coating detached. Finally, at loads greater than 30 N, gross spallation of the coating were observed, attributed to critical plastic deformation of the substrate.
- A reduction in the coefficient of friction (COF) of the materials was observed when performing the DUPLEX treatment. Additionally, instabilities in the COF due to critical plastic deformation were reduced. This produced a decrease in the worn volume and the amount of material accumulated on the edges of the scratch track, which in turn was reflected in the decrease of the wear coefficient between 21 and 31% after the application of the DUPLEX treatment.

Author Contributions: Conceptualization, Arturo Gomez-Ortega and Juan Manuel González Carmona; methodology, Christian Felix-Martinez, Guillermo César Mondragon-Rodríguez, Diego Germán Espinosa Arbelaez and Juan Manuel González Carmona; formal analysis, Arturo Gomez-Ortega, Julián Andrés Pinilla-Bedoya, Carolina Ortega-Portilla, Christian Felix-Martinez. Guillermo César Mondragon-Rodríguez, Diego Germán Espinosa Arbelaez, James Pérez-Barrera and, Juan Manuel González Carmona; investigation, Julián Andrés Pinilla-Bedoya, Carolina Ortega-Portilla; data curation, Arturo Gomez-Ortega and Juan Manuel González Carmona; writing—original draft preparation, Julián Andrés Pinilla-Bedoya, Carolina Ortega-Portilla and Juan Manuel González Carmona; writing—review and editing, Christian Felix-Martinez, Guillermo César Mondragon-Rodríguez, Diego Germán Espinosa Arbelaez, James Pérez-Barrera and Edgar Adrián Franco Urquiza; funding acquisition, Edgar Adrián Franco Urquiza. All authors have read and agreed to the published version of the manuscript."

Funding: This research was funded by CONAHCYT through the FORDECYT projects 297265 and 296384 and internal CIDESI project number QID0027. Materials for plasma nitriding and the AlCrN coating were partially provided through the CONAHCYT project 2015-02-1077 *Frontiers of Science*.

Data Availability Statement: The raw data supporting the conclusions of this article will be made available by the authors on request.

Acknowledgments: The authors thank the support provided by CONAHCYT through the FORDECYT program, support from national laboratory CENAPROT-CIDESI, and the Investigadores por México (previously Cátedras program) managed by CONAHCYT.

Conflicts of Interest: The authors declare no conflicts of interest.

References

1. L. Yang, K. Hsu, B. Baughman, D. Godfrey, F. Medina, M. Menon, S. Wiener, Additive Manufacturing of Metals: The Technology, Materials, Design and Production, Springer, 2017. https://doi.org/10.1007/978-3-319-55128-9
2. Ojestez Tripathi, Sashank Srivastava, Bharat Singh, Ankita Awasthi, S.K. Rajput, Pankaj Sonia, Piyush Singhal, Kuldeep K. Saxena. Powder bed fusion process in additive manufacturing: An overview. Riya Singh, Akash Gupta, Materials Today: Proceedings, 26 (2) (2020) 3058–3070. https://doi.org/10.1016/j.matpr.2020.02.635
3. I. Echeta, X. Feng, B. Dutton, R. Leach, S. Piano. Review of defects in lattice structures manufactured by powder bed fusion. Int. J. Adv. Manuf. Technol. 106 (2019) 2649–2668. https://doi.org/10.1007/s00170-019-04753-4
4. Adebola Adeyemi, Esther T. Akinlabi, Rasheedat M. Mahamood. Powder Bed Based Laser Additive Manufacturing Process of Stainless Steel: A Review. Materials Today: Proceedings 5 (9-3) (2018) 18510–18517. https://doi.org/10.1016/j.matpr.2018.06.193
5. Sanjeev K.C., P.D. Nezhadfar, C. Phillips, M.S. Kennedy, N. Shamsaei, R.L. Jackson. Tribological behavior of 17–4 PH stainless steel fabricated by traditional manufacturing and laser-based additive manufacturing methods. Wear. 440-441 (2019) 203100. https://doi.org/10.1016/j.wear.2019.203100
6. Bandar AlMangour, Jenn-Ming Yang. Improving the surface quality and mechanical properties by shot-peening of 17-4 stainless steel fabricated by additive manufacturing. Mater. Des. 110 (2016) 914–924. https://doi.org/10.1016/j.matdes.2016.08.037

7. M. Murayama, K. Hono, Y. Katayama. Microstructural evolution in a 17-4 PH stainless steel after aging at 400 °C. Metallurgical and Materials Transactions A. 30 (1999) 345–353. https://doi.org/10.1007/s11661-999-0323-2
8. H. Mirzadeh, A. Najafizadeh. Aging kinetics of 17-4 PH stainless steel. Materials Chemistry and Physics. 116 (2009) 119–124. https://doi.org/10.1016/j.matchemphys.2009.02.049
9. G.E. Hicho, J.H. Smith. Metallurgical evaluation of 17-4 PH stainless steel castings. NISTIR 89-4075 (1989). https://doi.org/10.6028/NIST.IR.89-4075
10. L.E. Murr, E. Martinez, J. Hernandez, S. Collins, K.N. Amato, S.M. Gaytan, P.W. Shindo. Microstructures and properties of 17-4 PH stainless steel fabricated by selective laser melting. Journal of Materials Research and Technology 1(3) (2012) 167–177. https://doi.org/10.1016/S2238-7854(12)70029-7
11. C. Zitelli, P. Folgarait, A. Di Schino, Laser Powder Bed Fusion of Stainless Steel Grades: A Review, Metals. 9 (2019) 731. https://doi.org/10.3390/met9070731
12. Qunli Zhang, Lijuan Wu, Hongsen Zou, Bo Li, Gang Zhang, Jingyong Sun, Jianjun Wang, Jianhua Yao. Correlation between microstructural characteristics and cavitation resistance of Stellite-6 coatings on 17-4 PH stainless steel prepared with supersonic laser deposition and laser cladding, J. Alloys Compd. 860 (2021) 158417. https://doi.org/10.1016/j.jallcom.2020.158417
13. G.C. Mondragón-Rodríguez, N. Torres-Padilla, N. Camacho, D.G. Espinosa-Arbeláez, G.V. de León-Nope 1, J.M. González-Carmona, J.M. Alvarado-Orozco. Surface modification and tribological behavior of plasma nitrided Inconel 718 manufactured via direct melting laser sintering method, Surf. Coat. Technol. 387 (2020) 125526. https://doi.org/10.1016/j.surfcoat.2020.125526
14. M. Tarnowski, T. Borowski, S. Skrzypek, K. Kulikowski, T. Wierzchoń. Shaping the structure and properties of titanium and Ti6Al7Nb titanium alloy in low-temperature plasma nitriding processes, J. Alloys Compd. 864 (2021) 158896. https://doi.org/10.1016/j.jallcom.2021.158896
15. P Kaestner, J Olfe, J.-W He, K.-T Rie. Improvement in the load-bearing capacity and adhesion of TiC coatings on TiAl6V4 by duplex treatment, Surf. Coat. Technol. 142-144 (2001) 928–933. https://doi.org/10.1016/S0257-8972(01)01214-2
16. Chun-Chi Chang, Jenq-Gong Duh. Duplex coating technique to improve the adhesion and tribological properties of CrAlSiN nanocomposite coating, Surf. Coat. Technol. 326 (2017) 375–381. https://doi.org/10.1016/j.surfcoat.2016.11.032
17. Hamidreza Riazi, Fakhreddin Ashrafizadeh, Sayed Rahman Hosseini, Reza Ghomashchi, Rong Liu. Characterization of simultaneous aged and plasma nitrided 17-4 PH stainless steel, Mater. Charact. 133 (2017) 33–43. https://doi.org/10.1016/j.matchar.2017.09.019
18. Carlos Eduardo Pinedo, Sharys Ivonn Varela Larrotta, Arthur Seiji Nishikawa, Hanshan Dong, Xiao-Ying Li, RodrigoMagnabosco, André Paulo Tschiptschin. Low temperature active screen plasma nitriding of 17–4 PH stainless steel, Surf. Coat. Technol. 308 (2016) 189–194. https://doi.org/10.1016/j.surfcoat.2016.07.096
19. Sandro D. Oliveira, André P. Tschiptschin, Carlos E. Pinedo. Simultaneous plasma nitriding and ageing treatments of precipitation hardenable plastic mould steel, Mater. Des. 28 (2007) 1714–1718. https://doi.org/10.1016/j.matdes.2006.03.011
20. H. Dong, M. Esfandiari. On the microstructure and phase identification of plasma nitrided 17-4PH precipitation hardening stainless steel, Surf. Coat. Technol. 202 (2008) 2969–2975. https://doi.org/10.1016/j.surfcoat.2007.10.036
21. Hamidreza Riazi, Fakhreddin Ashrafizadeh, Sayed Rahman Hosseini, Reza Ghomashchi. Influence of simultaneous aging and plasma nitriding on fatigue performance of 17-4 PH stainless steel, Materials Science and Engineering: A. 703 (2017) 262–269. https://doi.org/10.1016/j.msea.2017.07.070
22. P. Kochmański, J. Nowacki. Activated gas nitriding of 17-4 PH stainless steel, Surf. Coat. Technol. 200 (2006) 6558–6562. https://doi.org/10.1016/j.surfcoat.2005.11.034
23. S.D. Meredith, J.S. Zuback, J.S. Keist, T.A. Palmer. Impact of composition on the heat treatment response of additively manufactured 17–4 PH grade stainless steel. Materials Science and Engineering: A. 738 (2018) 44-56. https://doi.org/10.1016/j.msea.2018.09.066
24. M Pellizzari, A Molinari, G Straffelini. Thermal fatigue resistance of plasma duplex-treated tool steel. Surface and Coatings Technology, 142–144 (2001) 1109-1115. https://doi.org/10.1016/S0257-8972(01)01223-3
25. Niloofar Sanaei, Ali Fatemi, Nam Phan. Defect characteristics and analysis of their variability in metal L-PBF additive manufacturing. Materials & Design, 182 (2019) 108091. https://doi.org/10.1016/j.matdes.2019.108091
26. Mahmoud Naim, Mahdi Chemkhi, Julien Kauffmann, Akram Alhussein. Taguchi DoE analysis and characterization of 17-4 PH stainless steel parts produced by material extrusion (MEX) process. Advances in Industrial and Manufacturing Engineering 8 (2024). https://doi.org/10.1016/j.aime.2024.100138
27. Jörg Vetter, Wolfgang Burgmer, Anthony J. Perry. Arc-enhanced glow discharge in vacuum arc machines, Surf. Coat. Technol. 59 (1993) 152–155. https://doi.org/10.1016/0257-8972(93)90074-X

28. J.F. Archard, Contact and Rubbing of Flat Surfaces, J. Appl. Phys. 24 (1953) 981–988. https://doi.org/10.1063/1.1721448
29. Zhiheng Hu, Haihong Zhu, Hu Zhang, Xiaoyan Zeng. Experimental investigation on selective laser melting of 17-4PH stainless steel, Opt. Laser Technol. 87 (2017) 17–25. https://doi.org/10.1016/j.optlastec.2016.07.012
30. A. Kudzal, B. McWilliams, C. Hofmeister, F. Kellogg, J. Yu, J. Taggart-Scarff, J. Liang, Effect of scan pattern on the microstructure and mechanical properties of Powder Bed Fusion additive manufactured 17-4 stainless steel, Materials & Design. 133 (2017) 205–215. https://doi.org/10.1016/j.matdes.2017.07.047
31. R. Sowa, A. Kowal, E. Roga, S. Arabasz, A. Dziedzic, I. Dul, M. Parlinska-Wojtan, Influence of double solution treatment on hardness in 17-4 pH steel, Zaštita Materijala. 56 (2015) 261–268. https://doi.org/10.5937/ZasMat1503261S
32. Sudha Cheruvathur, Eric A. Lass, and Carelyn E. Campbell. Additive Manufacturing of 17-4 PH Stainless Steel: Post-processing Heat Treatment to Achieve Uniform Reproducible Microstructure. JOM, Vol. 68, No. 3, 2016. https://doi.org/10.1007/s11837-015-1754-4
33. Wee-Do Yoo, Jong-Hoon Lee, Kuk-Tae Youn, Young-Mok Rhyim. Study on the Microstructure and Mechanical Properties of 17-4 PH Stainless Steel depending on Heat Treatment and Aging Time. Solid State Phenomena Vol. 118 (2006) pp 15-20 doi:10.4028/www.scientific.net/SSP.118.15
34. Y Sun, T Bell, Low Temperature Plasma Nitriding Characteristics of Precipitation Hardening Stainless Steel, Surface Engineering. 19 (2013) 331–336. https://doi.org/10.1179/026708403225007545
35. F. Lomello, F. Sanchette, F. Schuster, M. Tabarant, A. Billard. Influence of bias voltage on properties of AlCrN coatings prepared by cathodic arc deposition, Surf. Coat. Technol. 224 (2013) 77–81. https://doi.org/10.1016/j.surfcoat.2013.02.051
36. Jian-Fu Tang, Ching-Yen Lin, Fu-Chi Yang, Yi-Jing Tsai, Chi-Lung Chang. Effects of nitrogen-argon flow ratio on the microstructural and mechanical properties of AlCrN coatings prepared using high power impulse magnetron sputtering, Surf. Coat. Technol. 386 (2020) 125484. https://doi.org/10.1016/j.surfcoat.2020.125484
37. C. Sabitzer, J. Paulitsch, S. Kolozsvári, R. Rachbauer, P.H. Mayrhofer. Impact of bias potential and layer arrangement on thermal stability of arc evaporated Al-Cr-N coatings, Thin Solid Films. 610 (2016) 26–34. https://doi.org/10.1016/j.tsf.2016.05.011
38. 38. Mohan Chen, Dongqing Wu, Wanglin Chen, Shihong Zhang. Structural optimisation and electrochemical behaviour of AlCrN coatings, Thin Solid Films. 612 (2016) 400–406. https://doi.org/10.1016/j.tsf.2016.06.032
39. E. Le Bourhis, P. Goudeau, M.H. Staia, E. Carrasquero, E.S. Puchi-Cabrera. Mechanical properties of hard AlCrN-based coated substrates, Surf. Coat. Technol. 203 (2009) 2961–2968. https://doi.org/10.1016/j.surfcoat.2009.03.017
40. T. Sampath Kumar, A. Vinoth Jebaraj. Metallurgical characterization of CrN and AlCrN physical vapour deposition coatings on aluminium alloy AA 6061, Materials Today: Proceedings. 22 (2020) 1479–1488. https://doi.org/10.1016/j.matpr.2020.01.506
41. Yu-ping Feng, Li Zhang, Rong-xian Ke, Qing-lei Wan, Zhe Wang, Zhi-hong Lu. Thermal stability and oxidation behavior of AlTiN, AlCrN and AlCrSiWN coatings, International Journal of Refractory Metals and Hard Materials. 43 (2014) 241–249. https://doi.org/10.1016/j.ijrmhm.2013.11.018
42. Nicholas X. Randall. The current state-of-the-art in scratch testing of coated systems, Surf. Coat. Technol. 380 (2019) 125092. https://doi.org/10.1016/j.surfcoat.2019.125092
43. P.A. Steinmann, Y. Tardy, H.E. Hintermann. Adhesion testing by the scratch test method: The influence of intrinsic and extrinsic parameters on the critical load, Thin Solid Films. 154 (1987) 333–349. https://doi.org/10.1016/0040-6090(87)90377-4
44. J.L. Mo, M.H. Zhu, B. Lei, Y.X. Leng, N. Huang. Comparison of tribological behaviours of AlCrN and TiAlN coatings—Deposited by physical vapor deposition, Wear. 263 (2007) 1423–1429. https://doi.org/10.1016/j.wear.2007.01.051
45. Sunil Kumar, Saikat Ranjan Maity, Lokeswar Patnaik. Friction and tribological behavior of bare nitrided, TiAlN and AlCrN coated MDC-K hot work tool steel, Ceram. Int. 46 (2020) 17280–17294. https://doi.org/10.1016/j.ceramint.2020.04.015

Disclaimer/Publisher's Note: The statements, opinions and data contained in all publications are solely those of the individual author(s) and contributor(s) and not of MDPI and/or the editor(s). MDPI and/or the editor(s) disclaim responsibility for any injury to people or property resulting from any ideas, methods, instructions or products referred to in the content.